Chupakhin, S.; Klusemann, B.; Huber, N.; Kashaev, N.:
Application of design of experiments for laser shock peening process optimization.
In: The International Journal of Advanced Manufacturing Technology. Vol. 102 (2019) 5-8, 1567 - 1581.
First published online by Springer: January 09, 2019

DOI: /10.1007/s00170-018-3034-2
https://dx.doi.org/10.1007/s00170-018-3034-2

Application of design of experiments for laser shock peening process optimization

Sergey Chupakhin[1], Benjamin Klusemann[1,2], Norbert Huber[1] and Nikolai Kashaev[1]

[1]Institute of Materials Research, Materials Mechanics, Helmholtz-Zentrum Geesthacht, Geesthacht 21502, Germany
[2]Institute of Product and Process Innovation, Leuphana University of Lüneburg, Lüneburg 21335, Germany

Corresponding author:
Sergey Chupakhin, Helmholtz-Zentrum Geesthacht, Max-Planck-Str 1, 21502 Geesthacht, Germany.

Email: sergey.chupakhin@hzg.de
Phone: +494152872637

Abstract

The aircraft industry requires new cost efficient approaches for the life extension, repair, and maintenance of the growing fleet of ageing aircrafts. In this regard, laser shock peening — a very promising life enhancement technique — has already demonstrated great success regarding the improvement of fatigue behavior via deep compressive residual stresses. However, the prediction and adaption of residual stress fields on basis of the laser peening parameters is still not comprehensively established. In the present work, effects of the laser pulse energy, the number of treatment overlaps as well as the treatment spot size on the resulting residual stresses are investigated. In particular, the residual stress close to the surface, the maximum compressive residual stress and the integral stress area over the specimen depth represent key properties for application of laser peening. For the systematic investigation of all main and interaction-based process parameter effects, and subsequent parameter optimization, the general full factorial design is employed. The generated residual stresses measured by hole drilling require correction due to plasticity effects. This correction is performed based on a previously developed artificial neural network methodology. The results show, that laser shock peening with different process parameter combinations, which induce the residual stresses with comparable integral stress area, can lead to a minimum fatigue life extension of approx. 100000 cycles. The experimental scatter in the number of cycles to failure follows the Weibull distribution which qualitatively correlates with the standard deviation of the integral stress area.

Keywords

Laser shock peening, residual stress, design of experiments, hole drilling, fatigue crack growth.

1. Introduction

There is a strong economic motivation of industrial companies to explore novel approaches of fatigue life extension due to the limitations of existing surface modification techniques regarding

the residual stress maximum depth and geometrical restrictions of the treated structures, such as the holes or flat surfaces. One promising approach is laser shock peening (LSP), which has already demonstrated great success in regard to the mitigation of fatigue crack growth [1—6], but is not comprehensively established in terms of quantitative prediction of fatigue behavior. The following sections summarize the state of art of the LSP process, results achieved under high-cycle fatigue and fatigue crack propagation, and process optimization.

Laser shock peening

LSP induces compressive residual stresses deep into the material, which can significantly increase fatigue life, especially in cases where damage is caused by a crack initiated at the surface [7—8]. In comparison to conventional techniques, LSP has many advantages [1], such as flexibility in processing different geometries and capability of use in existing production lines, low surface roughness, and a controllable laser pulse beam with the possibility to strengthen the material at the corners. LSP is a clean and sustainable process with no need for material recycling unlike shot peening.

The LSP process and a typically induced residual stress distribution are schematically shown in Fig. 1. A laser with high-pulse energy is used for treatment of the material surface, which is usually covered by a water-confining layer. Having passed through water, the laser beam is absorbed by the material, which turns into plasma. Consequently, the plasma expands very rapidly by absorbing the laser energy during the pulse. The transparent water layer traps the plasma, causing a high pressure at the material surface. The energy of the high-pressure plasma partially turns into mechanical shock waves, which propagate deep into the material. These high-pressure shock waves lead to generation of deep compressive residual stresses underneath the treated area and typically tensile stresses in the surrounding areas [1, 9]. Similar to cold working mechanisms LSP treatment increases the material hardness in the peened area [10].

LSP has been adopted by many companies such as Toshiba, Rolls-Royce, Metal Improvement Company, LSP Technologies, Boeing, U.S. Air Force, etc. [11—15]. However, the fatigue life extension of treated components is not precisely defined; i.e. only a rough (and usually not reproducible) estimation of a number of cycles until failure of the structures is provided. This is mostly attributed to the lack of knowledge regarding the prediction and control of residual stress profiles in dependence on the LSP parameters.

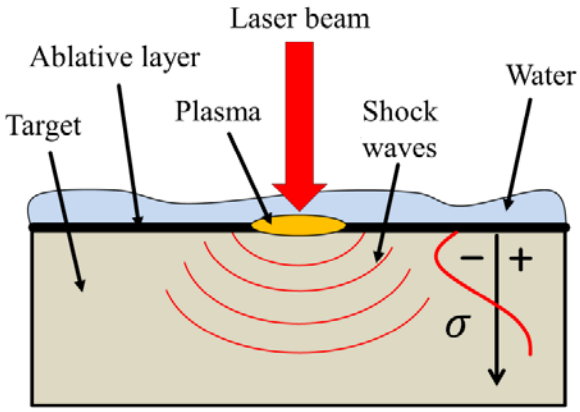

Fig. 1 LSP process. Depicted and adopted according to [1, 8]

High-cycle fatigue

The influence of residual stresses generated by the LSP on the fatigue life was investigated by Correa et al. [16] and Bhamare et al. [17]. Correa et al. [16] have demonstrated fatigue life extension due to the LSP treatment up to 243%, depending on a sequence of the LSP pulses on the specimen surface. It was shown that the crack is always initiated at the specimen surface and then propagates through the thickness of the specimen, following a thumbnail-shaped pattern that matches the residual stress profile. The compressive residual stress acting opposite to the externally applied load suppresses the crack growth, while the tensile stress speeds it up. Fatigue life extension was mainly achieved due to the prevention of the crack nucleation, which is attributed to subsurface compressive stresses. On the other hand, specimens with subsurface tensile stresses after LSP do not demonstrate life extension, even if high compressive stresses are present in the body of the specimen. The tensile stresses promote crack propagation at higher rates, following the thumbnail pattern. Therefore, the magnitude of the subsurface stress is considered to be more important than actually the integral or average stresses through the thickness.

Fatigue crack propagation

Much research has been carried out regarding the mitigation of fatigue crack growth via the residual stresses generated by LSP [4—6, 18, 19]. Depending on the LSP process parameters and the resulting residual stress field inside the material, the fatigue life of treated specimens was increased by a factor of 10 relative to untreated specimens. The crack arrest is attributed to entering the region with higher compressive residual stresses [18]. In the LSP treated area, the occurrence of micro-fatigue-steps and secondary cracks contribute to the retardation of the crack growth. The through-thickness striations on the fracture surface of the thin specimen are formed parallel to the crack growth direction indicating the retardation regions. The secondary cracks appear between the fatigue striations at any depth of the material. Furthermore, a through

thickness compressive stress profile demonstrates higher fatigue performance in comparison with only a subsurface compressive stress layer as produced by conventional shot peening [20]. This phenomenon is attributed to the fatigue crack closure due to the presence of compressive residual stresses as well as the generation of secondary cracks and the local stress redistribution, causing a misorientation during the crack propagation.

Laser shock peening process optimization

Over the last three decades, large amount of research has been accomplished regarding the LSP process optimization [17, 21, 22]. The generation of desired residual stress fields by controlling the laser parameters has always been one major objective. The LSP process can be described in four stages: (i) delivery of the laser beam with a defined energy; (ii) plasma generation on the surface of the material under the confining medium; (iii) propagation of the high-pressure waves in the material; (iv) plastic deformation and generation of residual stresses inside the material. Regarding the first stage, the current market offers different pulsed laser systems with a pulse duration of nanoseconds and energy of 10 J, which meet the LSP objectives.

As for the second stage, the measurement of plasma parameters is very challenging due to the extremely short process duration (nanoseconds) and high energies [1, 23]. Spectroscopic techniques for the determination of plasma temperature and density cannot be used because the water layer is not transparent for the emitted radiation [1].

At the next stage, the shock waves propagating into the material also have a duration in the order of nanoseconds and attenuate during the propagation. The “locked-in” nature of these shock waves of high pressure makes it very challenging to measure them as well. On experimental basis this brings a significant amount of inaccuracy concerning the prediction of generated residual stresses without detailed information about the original cause.

Because of the measurement difficulties described above, modeling gained large attention in recent years [24—26]. Many studies in this field have been accomplished with the aim of creating an FEM model for the simulation of shock wave propagation and the generation of resulting residual stresses. The boundary conditions of the FEM model can be calibrated using the back free surface velocities behind thin specimen foils and shock yield strengths measured by VISAR (Velocity Interferometer System for Any Reflector) Doppler velocimetry [27]. In these cases, the validation of FE simulation is provided by the comparison of the resultant simulated and experimental LSP-induced residual stress profiles.

Finite Element simulations helped to understand the LSP process. However, high computational costs, model assumptions and uncertainties in measurement techniques limits their application. Therefore only a qualitative assessment of the induced residual stresses is possible. For

establishing quantitative process properties relationships, experiments are still the only reliable access.

In the light of the described challenges, researches have utilized statistical design of experiments (DOE) techniques for systematic LSP optimization [28—32]. The main advantage of DOE is that it does not require knowledge about the plasma generation and shock-wave propagation, i.e. the intermediate stages of the LSP process are considered as “black box”, represented by the experiments in which material properties, LSP process parameters and resultant residual stresses are handled. Trdan et al. [32] investigated the influence of the laser pulse density on the surface roughness, subsurface residual stresses at a depth of 0.03 mm, microhardness, and corrosion resistance for the two aluminum alloys AlMgSiPb and AlSiMgMg. The performed DOE revealed a strong relationship between the laser pulse density and the intensity of pitting corrosion attack as well as the subsurface stress. The optimum laser energy was achieved for sufficient enhancement of surface modification process in terms of surface roughness, corrosion resistance and microhardness of the treated material.

Most recently, Ebrahimi et al [30] investigated the effects of the laser intensity, laser spot size and overlapping amount of shot spacing on corrosion and hardness properties of ANSI 316 stainless steel. DOE was utilized to identify these main effects and their interactions of LSP parameters to predict the corrosion and hardness for inaccessible input combinations. The results reveal that both corrosion resistance and surface hardness are improved by maximum of 100% and 35%, respectively, by increasing the laser spot size and laser intensity. With the help of DOE it was found that hardness is more strongly related to the laser intensity while the corrosion resistance is mostly depended on the amount of shot overlapping.

Cellard et al. [28] performed an investigation of the influence of LSP parameters on the mechanical parameters of titanium alloy Ti-5Al-2Sn-2Zr-4Cr-4Mo (Ti-17). The specimen thickness, laser pulse energy and duration, number of impacts were controlled parameters while the residual stress averaged at a depth of 4μm under the surface, Vickers microhardness, the specimen curvature, and the width of the diffraction peaks represent the measured output variables. The achieved results demonstrate that all parameters influence the sample curvature, while the integral width is only affected by the pulse duration. The roughness of titanium alloy is maintained constant in all experiments and is therefore not influenced by any of the process parameters. The thickness affects the residual stress profile — the tensile stresses occurred at the surface of the specimens with the thickness of 5 mm, but in case of 45 mm thickness compressive stresses were found at the surface. DOE analysis revealed interaction effects of thickness/pulse density and pulse duration/pulse density on microhardness which would have not been possible to determine by running of one-factor-at-a-time experiments.

The effect of LSP, working at 10 kHz repetition rate, pulse duration of 14 ns, and the laser power of 3.52 W on magnesium based biodegradable alloys was recently investigated by Kamkarrad et al. with the help of DOE techniques [31]. In this work the laser intensity, number of shots and percentage of overlap were considered as controllable parameters and the maximum peening depth, surface roughness, and microhardness were considered as measured parameters. DOE analysis provided the threshold values of controllable LSP parameters, which refer to 2 GW/cm^2, leading to a significant increase in surface roughness and microhardness.

In studies mentioned above the influence of laser shock peening process parameters on material surface roughness, material microhardness, corrosion resistance, and subsurface residual stresses is investigated. Unlike these studies, the present work employs DOE analysis for the LSP process optimization in regard to generated residual stress profiles over the depth of AA2024-T3 specimens. More precisely, the shape of the stress profile and the subsurface stress are considered as an object of optimization in order to simultaneously improve the fatigue and fatigue crack propagation behaviors.

2. Material and methods

2.1 Material

AA2024-T3 is an advanced aluminum alloy mostly used in the aerospace industry, possessing excellent fatigue resistance, high fracture toughness, and high formability [33]. Due to its high strength-to-weight ratio, AA2024-T3 leads to a good damage tolerance behavior of aircraft structures. It is a high-strength material of adequate workability and has also excellent ductility, which decreases not significantly under the strengthening heat treatment [34—36]. Moreover, it has good machinability and surface finish capabilities. Annealing of AA2024 is performed at a temperature of 413 °C, leading to a yield strength of 370 MPa, an ultimate tensile strength of 490 MPa, a Young's modulus of 73.1 GPa, and strain at fracture of 16% [37].

2.2 Laser shock peening

The illustration of the LSP process is presented in Fig. 2. The Q-switched Nd:YAG laser works at a maximum frequency of 10 Hz. The pulse duration can be switched between 10 ns and 20 ns. The material surface is covered with a laminar water layer, used as confining medium for the plasma. Specimens produced from AA2024-T3 sheets of 2 mm thickness are treated with laser pulses sequentially along the path as shown in Fig. 2. The laser beam is focused on the surface as a square spot using an optical system. Two different optics of 1×1 and 3×3 mm^2 are used in the experiments. For generating very deep compressive stresses an up to five times 100% overlap of the laser spot is applied.

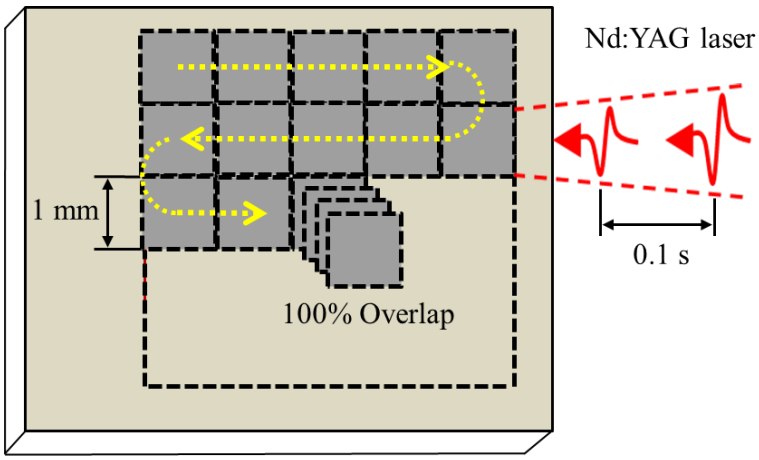

Fig. 2 Schematic illustration of the LSP process. Depicted and adopted from [38]

2.3 Hole drilling

The hole drilling system Prism from Stresstech company equipped with an optical electronic speckle pattern interferometer (ESPI) was used for measurement of residual stresses [39—42]. It captures high-quality full-field surface relaxation data during incremental hole drilling in order to accurately determine the originally existing residual stresses based on the integral method. The hole drilling approach has attracted a lot of attention in different industrial applications due to its high reliability, relatively low cost, high accuracy, and — at the same time — mostly tolerable damage to the workpiece.

However, as measuring residual stresses approaching the material yield strength, local plastic deformation occurs near the boundary of the hole as a result of the notch effect, which causes significant deviation from the assumed material linearity [43, 44]. The Integral method, used for back-calculation of residual stresses, assumes a linear elastic material behavior, thus the stress determination error arises as soon as local plastic deformation occurs. Chupakhin et al [38] have investigated the effect of plasticity for LSP-shaped stress fields by employing finite element modelling and artificial neural networks. The developed methodology allows the correction of non-uniform residual stress profiles for a wide range of material behavior and stress levels. It was demonstrated that, besides of the stress level, the stress shape in combination with the depth of maximum stress values strongly influences the amount by which the actual residual stress is overestimated in dependence of depth. Resulting measurement errors can reach more than 100%, if they are not corrected. It was also shown, that the LSP-shaped equibiaxial residual stresses below 80% of the yield strength do not require a correction and can be reliably determined by the hole drilling. In this case the error is below 10%.

2.4 Design of experiments

The exploration of a process property relationship can be achieved by conducting experiments in a systematic manner. The development of an experimental strategy that minimizes resource usage and yields the maximum knowledge requires tools involving statistical methods such as DOE [45—48]. Especially for processes that cannot be accurately enough described by simulations, the experimental design techniques are very important.

As mentioned in the introduction the subsurface residual stresses in the material have a strong effect on the fatigue behavior of thin-walled structures, while the fatigue crack propagation behavior is significantly influenced by the through-thickness residual stress profile. Therefore, the LSP parameters should be optimized in regard to desired residual stresses, which simultaneously enhance fatigue and fatigue crack growth life. Therefore, the responses attributed to the LSP-generated residual stress profiles were defined as follows: *stress at 0.01* mm ($S_{0.01}$) depth, *maximum stress* (S_{max}) depth, and the integral *stress area* (S_A) under the stress curve. The responses are schematically presented in Fig. 3.

The relevant factors that have an effect on residual stress distribution and directly define the cost of LSP performance are the following: the *energy* of the laser pulse, the number of LSP *overlaps*, and the focusing *optics*. They are schematically illustrated in Fig. 4. The laser energy levels are defined as 1.3, 3, and 5 J in order to cover the range of pulse energy of the current LSP facility. Square optics 1 and 3 mm with areas of 1 mm^2 and 9 mm^2 respectively, are used. The number of overlaps varies from one up to three times, which is typically used in industrial applications with energies of up to 5 J and a frequency of 10 Hz.

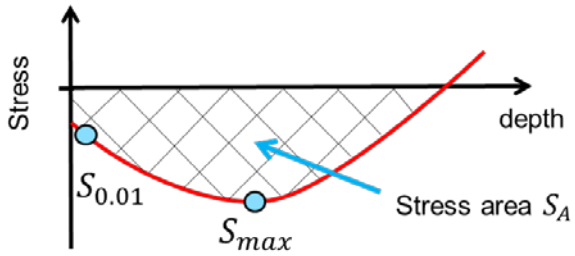

Fig. 3 Response variables related to the LSP-induced residual stress profile

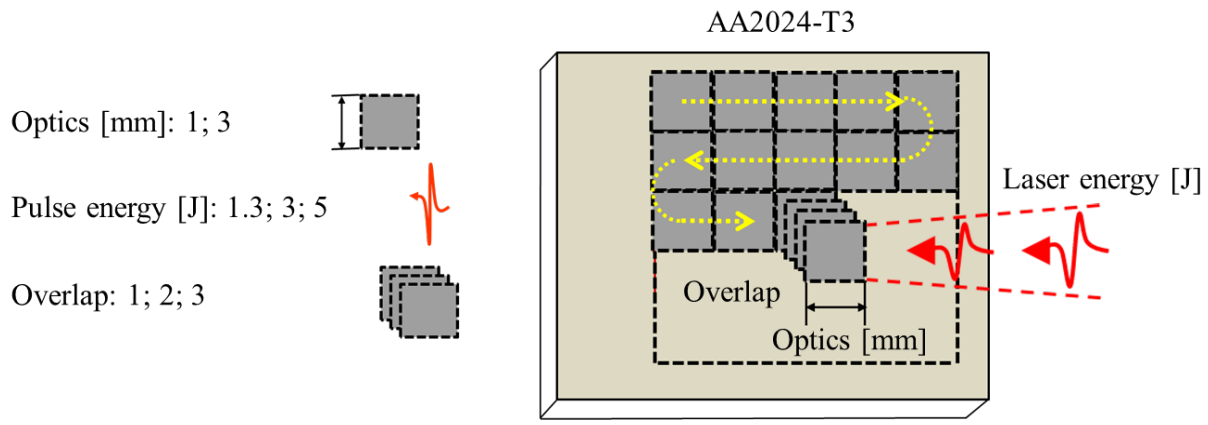

Fig. 4 Factor variables related to the LSP process

The general full factorial design is employed for the systematic investigation of all main and interaction-based factor effects. The combinations of factor levels, consisting of 18 unique runs, are replicated three times in order to enhance the ability of the DOE to determine the factor effects. In total, 54 experiments were designed. The DOE study was performed using the software ReliaSoft DOE++ [49].

3. Optimization of laser shock peening process

3.1 DOE: planning stage

The designed 54 experiments of the LSP treatment were conducted in random order to exclude the bias in the response variables and a systematic error associated with the specific factor combinations [50, 51]. The generated residual stresses in the specimens were measured by the hole drilling technique and designed responses were calculated. The information about the factor and response variables as well as the run order of the experiments are listed in Table 4. Four out of the 54 treatments were failed to measure because of the low surface reflectivity after LSP and they are marked with "-". The power study, i.e. the probability of determining an effect of the factor or factor combinations on the responses, if any [50, 51], for planned and performed experiments is presented in Table 1. In this work, an acceptable probability level for the factor effect detection was defined as 80%. Table 1 shows that the originally planned experiments have sufficient determination ability for the main effects and two-way interaction A•B and A•C, while the B•C as well as three-way interaction A•B•C are unlikely to be determined correctly from the planned experiments and should be considered with caution. Due to the failure of some experiments, the power for factor effects has dropped slightly, but it is still considered acceptable within the framework.

Table 1 Design evaluation: power study

Factor and interaction	Power for effect, planned experiments	Power for effect, performed experiments
A: Optics	0.9754	0.9635
B: Overlap	0.8354	0.7928
C: Energy	0.9048	0.8843
A • B	0.8354	0.7928
A • C	0.9048	0.8843
B • C	0.1	0.1
A • B • C	0.1	0.1

3.2 DOE: analysis of the response *stress at 0.01 mm*

The identification of main and interaction effects of the factors on the response *stress at 0.01 mm* ($S_{0.01}$) is presented in this chapter in order to demonstrate the significance of the regression model fitted into the experimental data.

An indicator of the acceptance of the regression model for the data-fitting is the T-value [46, 50, 51]. The T-value is defined by a statistical hypothesis test and it characterizes the effect of a factor or factor interaction on a response, i.e. how significantly the term influences a response in the presence of other terms.

The factor screening for the response *stress at 0.01 mm* is presented in Fig. 5a). The statistical test shows that all main factor effects A, B, and C and interactions B•C and A•B are significant. In general, three-way interactions rarely occur; as expected here, A•B•C is negligible. The T-value of the interactions A•B, B•C slightly exceeds a critical value of 1.68, which means that these interactions are not strong; therefore, the main factor effects A, B, C can be considered separately according to their importance. Moreover, B•C may contain inaccuracies due to the structure of design, as shown in the power study. *Optics* and *energy* have no interaction with respect to the residual stress under the surface when the number of *overlaps* is fixed.

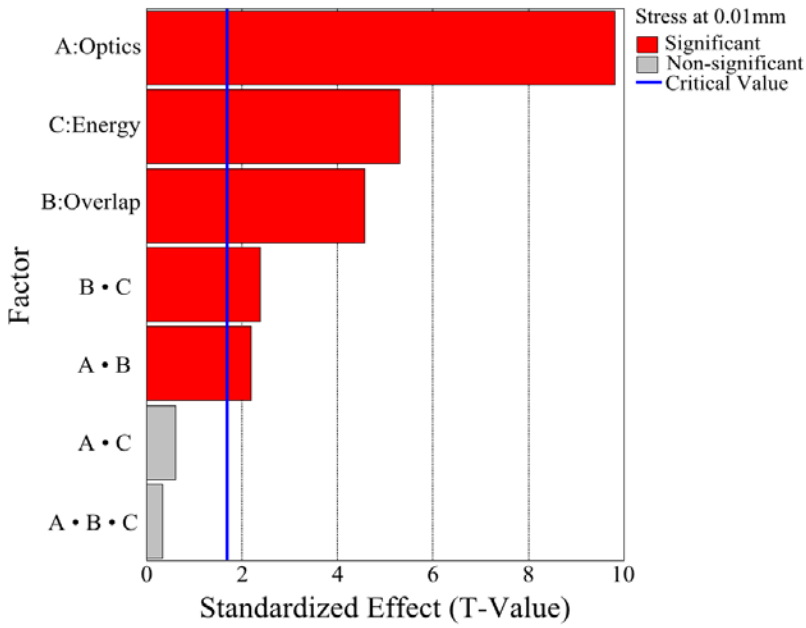

(a)

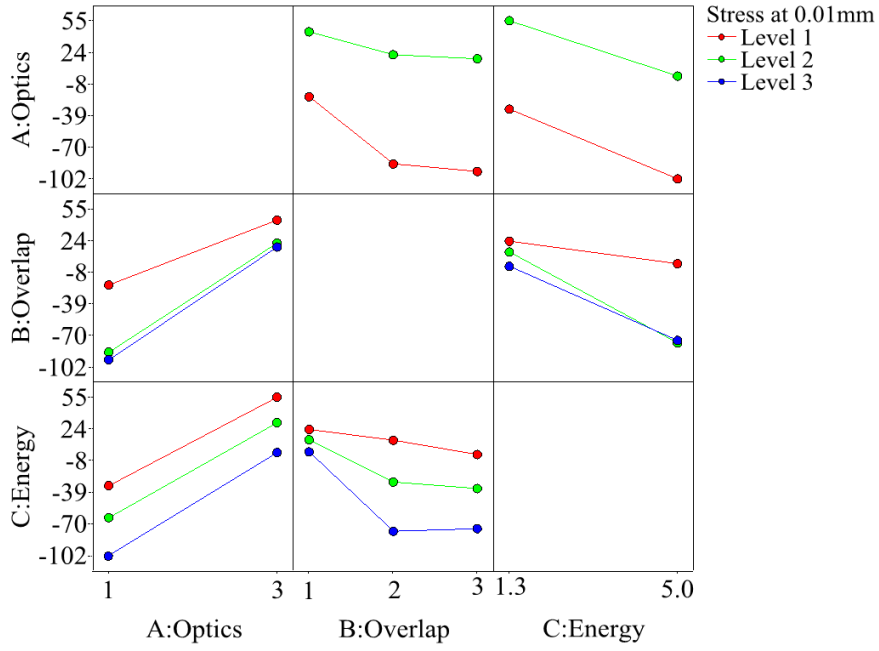

(b)

Fig. 5 *Stress at 0.01 mm* response: (a) factor screening, (b) factor interaction effects

The interaction effects are presented in Fig. 5b). Factor points corresponding to the fitted regression model are connected with the lines. On the plot, when any two factors are addressed the third factor is considered as the least square approximation of its levels. The lines — which are not parallel — intersect. The intersecting angle reflects the strength of interaction between

different factors. B•C and A•B interactions seem to have comparable significance, as seen already by the statistical test.

The model variability — i.e. how well the regression model fits the experimental data — is determined by the R^2 factor [46, 50—52]. Factor R^2 is 81.49% for the regression model of *stress at 0.01 mm* response, which exceeds the acceptance level of 80% defined in this work.

For the examination of the influence of the o*verlap* and *energy* variations on the s*tress at 0.01 mm*, the *optic* is kept at 1 mm, the results are shown in Fig. 6 [52]. The isolines show the factors variations which correspond to the desired *stress at 0.01 mm* value. The response surface is nearly symmetric to the vertical plane passing through the maximum and minimum response values on the graph. This means that both *overlap* and *energy* have almost equal significant effects and little interaction effect on the *stress at 0.01 mm*, as already inferenced in the statistical test. *Stress at 0.01 mm* decreases by increasing either *overlap* or *energy* and reaches its minimum, i.e. maximum compressive stress, when the factors are at their maximum values and vice versa. What follows is that the *stress at 0.01* can reach low values by increasing the number of *overlap*, when operating with relatively low *energy*. Thereby, the laser price, which is defined by the laser power, can be decreased; however, on cost of an increasing processing time.

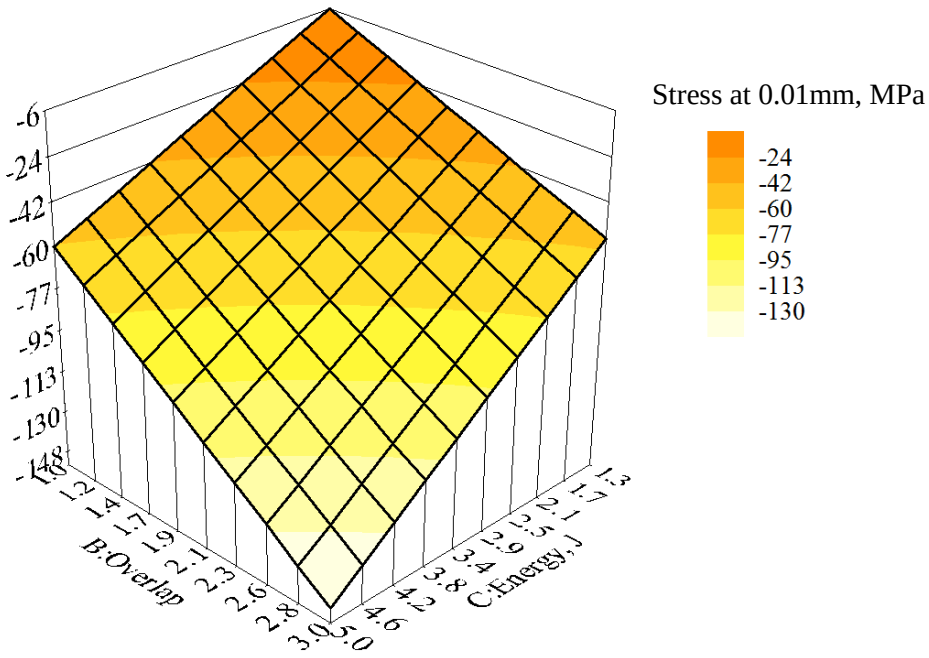

Fig. 6 *Stress at 0.01 mm* response as a function of overlap and energy factors

3.3 DOE: LSP process optimization

In Fig. 7, the *stress area* is plotted over *energy* and *overlap*, using a 1 mm *optics*. The feasible regions of *energy* and *overlap* variation corresponding to a *stress area* more negative than −200 MPa mm, −230 MPa mm, −250 MPa mm, and −290 MPa mm are illustrated in Fig. 7. The orange curve shows the least factor values that provide the given *stress area* value and thereby divides the plot into two parts. The curve is almost linear and diagonal, which shows the equal factor significance, i.e. for achieving desired *stress area*, either *energy* or *overlap* can be varied. A *stress area* up to −250 MPa mm can be achieved by increasing the number of *overlap* and keeping the *energy* at its minimum. Therefore, in order to generate the desired *stress area* value, one can adjust the *energy* and *overlap* levels based on the available laser energy and the cost of one LSP shot (one overlap). To reach a *stress area* of −290 MPa mm the maximum factor's levels, 5 J, 3 overlap, have to be applied.

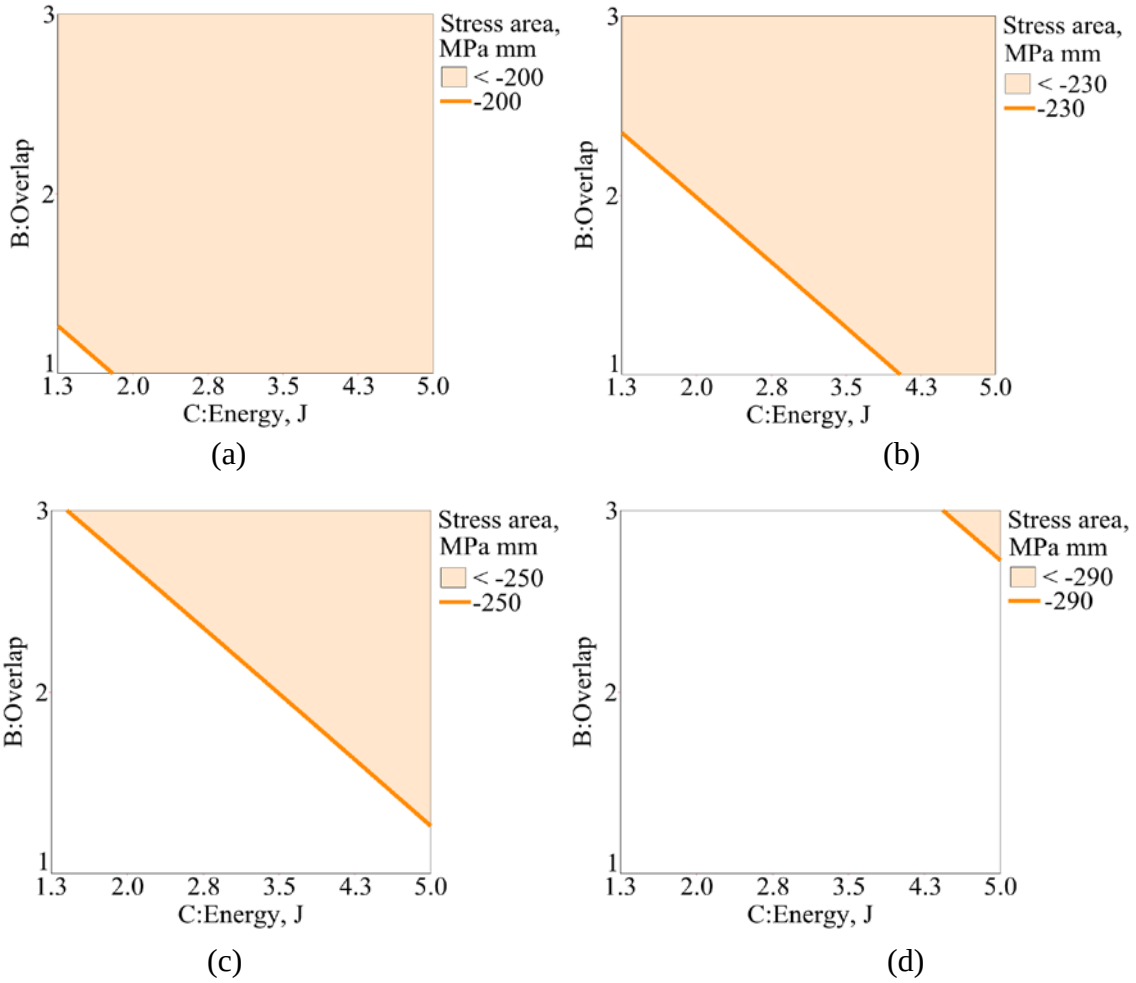

Fig. 7 Feasible range of the *energy* and *overlap* variation for achieving: (a) *stress area* < −200 MPa mm, (b) *stress area* < −230 MPa mm, (c) *stress area* < −250 MPa mm, (d) *stress area* < −290 MPa mm. *Optics* is 1 mm for all cases

Fig. 8 presents the *stress area* as a function of *energy* and *overlap* using a 3mm *optics*. The feasible regions of the *energy* and *overlap* variation corresponding to the *stress area* more negative than −20 MPa mm, −70 MPa mm, −130 MPa mm and −200 MPa mm are illustrated in Fig. 8. All plots demonstrate higher influence of the *energy* on the response than the *overlap* as the isoline has a curvature. Again, a maximum *stress area* of −200 MPa mm requires using maximum energy of 5 J and 3 overlap. For the configuration of the study when comparing Fig. 7 (for 1 mm *optics*) and Fig. 8 (for 3 mm *optics*), −200 MPa mm represents the limit for 3 mm *optics*. For higher values of the *stress area* 1mm *optics* has to be used.

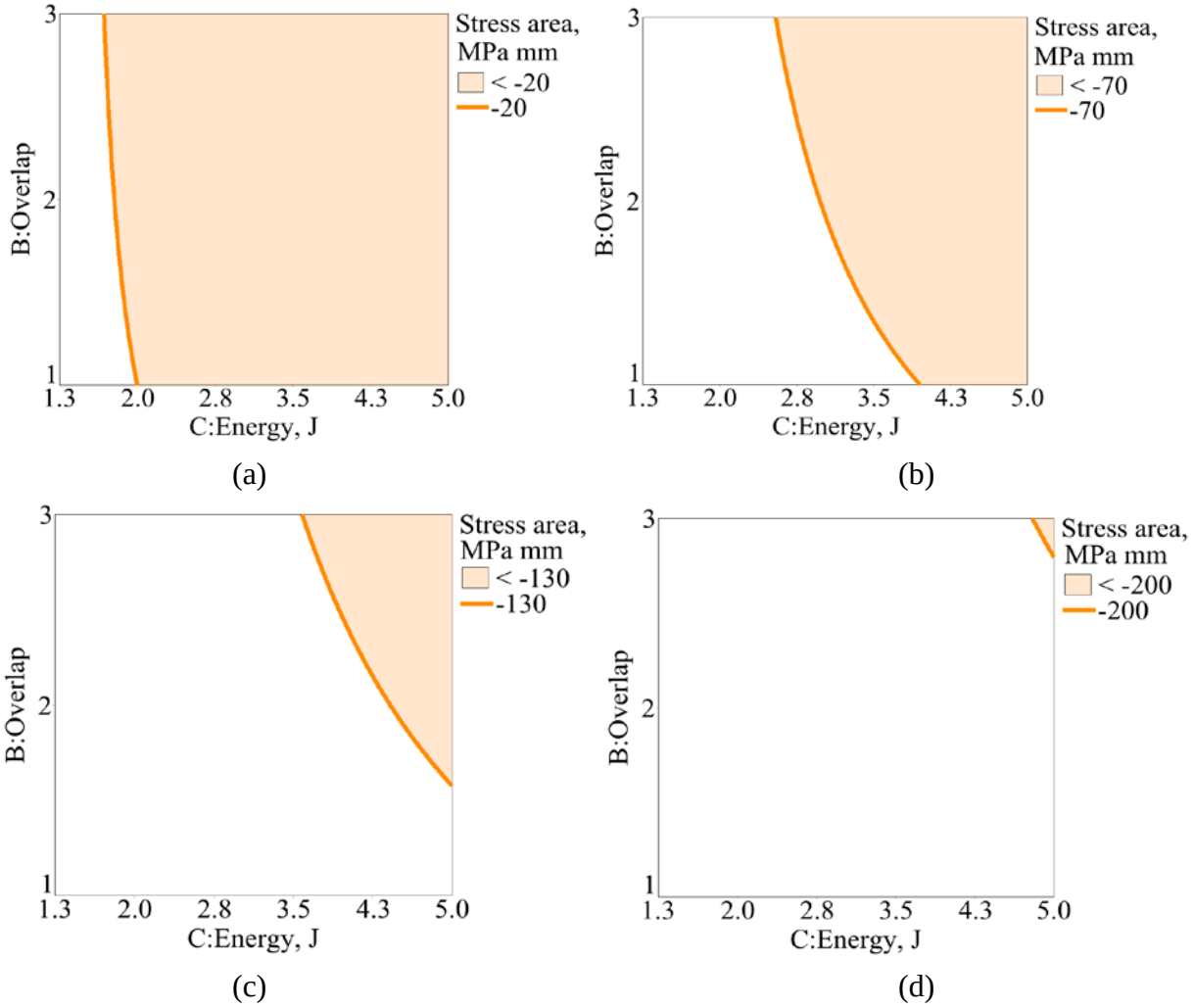

Fig. 8 Feasible range of the *energy* and *overlap* variation for achieving: (a) *stress area* < −20 MPa mm, (b) *stress area* response < −70 MPa mm, (c) *stress area* < −130 MPa mm, (d) *stress area* < −200 MPa mm. *Optics* is 3 mm for all cases

The optimization of *energy* and *overlap* for 1 and 3 mm optics was performed in regard to *stress at 0.01 mm* and *maximum stress* responses. In Fig. 9a), b) the *stress at 0.01 mm* and *maximum stress* are plotted in dependence of the *overlap* and *energy* for 1 and 3 mm optics, respectively.

In Fig. 9a) the green and orange curves show the least factor levels that provide the *stress at 0.01 mm* of −100 MPa and the *maximum stress* of −300 MPa, respectively. The region of *energy* and *overlap* variation corresponding to the *maximum stress* values more negative than −300 MPa fully covers the region of factor variation for *stress at 0.01 mm* values more negative than −100 MPa. The feasible region of *energy* and *overlap* variation lies between 3.1–5.0 J and two to three times overlaps. As shown in Fig. 9b) the 3 mm *optics* is capable of providing only the *stress at 0.01 mm* of −20 MPa by adjusting the *energy* and *overlap* to their highest levels of 5 J and three times, respectively.

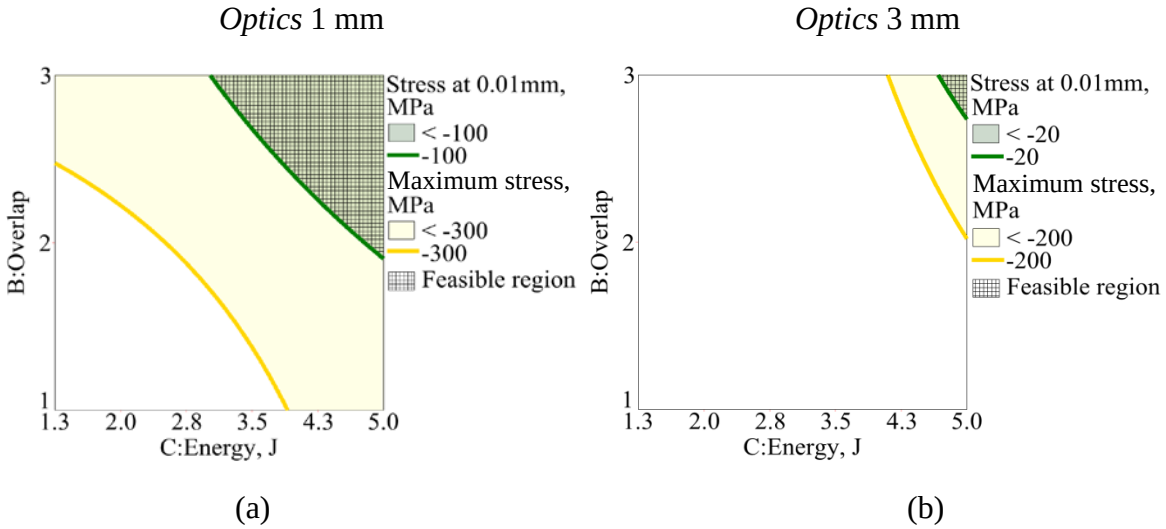

Fig. 9 Feasible range of the *energy* and *overlap* variation for achieving: (a) *stress at 0.01 mm* < −100 MPa, *maximum stress* < −300 MPa, *optics* 1 mm, (b) *stress at 0.01 mm* < −20 MPa, *maximum stress* < −200 MPa, *optics* 3 mm

The optimization of all residual stress responses for a 1 mm *optics* is presented in Fig. 10, where the s*tress area*, s*tress at 0.01 mm* and *maximum* s*tress* are plotted vs. *overlap* and *energy*. The feasible region of all factors variation is equal to the acceptable region for s*tress at 0.01 mm.* This means that within the investigated factor variations, the highest effort is required for achieving the desired *stress at 0.01 mm* compared to other responses.

As shown in Fig. 10, the acceptable region of factor variations, corresponding to *maximum stress* values more negative than −300 MPa, covers the regions of factor variations for other stress responses. According to the feasible region, one can operate with minimum *energy* of 3.1 J and three times *overlap* (P_1) or maximum *energy* of 4.8 J and two times *overlap* (P_2). In terms of processing time this implies an increase by 50% by working with the lower energy. It should be mentioned that operating with 1mm *optics* increases the processing time by the factor of 9 comparing with the 3 mm *optics* in accordance with the treated areas, however, in this case involving a change in the residual stresses.

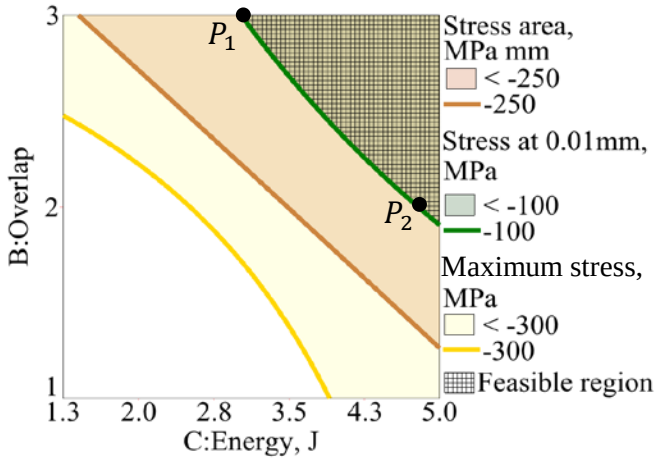

Fig. 10 Residual stress responses optimization: the feasible range of the *energy* and *overlap* variation for 1 mm *optics*

3.4 Correction of measured residual stress profiles

As mentioned above, the hole drilling yields an error in residual stress determination when measuring LSP-shaped residual stresses approaching 80% of material yield strength. Therefore, all residual stress profiles are subjected to the stress correction using the artificial neural network methodology established by Chupakhin et al. [38] in the following. After the correction the neural network returns the actual stress profile after evaluating the possible effect of plastic deformations. The stress profiles affected by nonlinearity are corrected and those which are not affected are left unchanged.

Out of 50 experimental observations, 10 (20%) were corrected by the neural network approach, while all others remained unchanged. The required correction in the measured stress profiles (characterized by stress responses) and the corresponding LSP parameters are listed in Table 5. After correction, the absolute values of the *stress area* and of the *maximum stress* are decreased by 15%. The *stress at 0.01 mm* did not require any correction and therefore, it remained unchanged. Moreover, 15% stress correction is comparable with 10–20% measurement error of the hole drilling equipped with ESPI and is considered to be not significant when carrying out a single measurement. However, in the current work, the DOE is performed where a relationship between factor and response variables is obtained from carefully planned experiments using statistical methods. Thus, the measurement error is considered by the regression model when predicting new observations. Therefore, the performed DOE is enhanced by including the correction of the measured stress profiles obtained through the ANN methodology. The minimum compressive *maximum stress* changed from −359 MPa to −332 MPa and the minimum *stress area* from −298 MPa mm to −265 MPa mm.

The corrected values are plotted over the *overlap* and *energy* for the now corrected regression model in Fig. 11. As shown, the *stress at 0.01 mm* and *stress area* acceptable regions are almost identical after correction; they build up a feasible region of all responses. This means that after

correction of stress profiles, in particular *stress at 0.01 mm* and *stress area* — which directly influence the fatigue and fatigue crack propagation, respectively — require comparable effort for achieving the desired values.

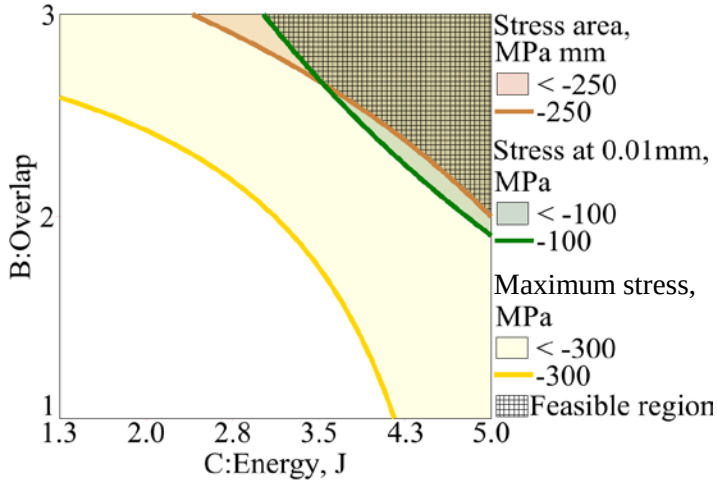

Fig. 11 Residual stress responses optimization: the feasible range of the *energy* and *overlap* variation, 1 mm *optics* for the neural network corrected data

4. Application of laser shock peening for improvement of fatigue resistance

The two process parameter combinations — *energy* of 3.1 J and three times *overlap* (P_1) — and — e*nergy* of 4.8 J and two times *overlap* (P_2) — represent the minimum and maximum laser pulse energy from feasible region achieved in DOE study to obtain the desired residual stress properties. Accordingly to the regression model these parameters lead to generation of residual stress profiles with comparable integral stress area and therefore were selected for the demonstration of fatigue behavior of the C(T)50 specimens.

The illustration of the C(T)50 specimen with the sequence of the LSP spots is presented in Fig. 12. LSP without coating was performed using a Q-switched Nd:YAG laser operating at 10 Hz with a pulse duration of 10 ns. A 1×1 mm diffractive square optics is used. The C(T)50 specimens were LSP treated from one side. The specimens had been “pre-cracked” 2 mm from the original crack length $a_0 = 10$ mm, thus the crack tracking starts from $a_0 = 12$ mm. The pre-crack was performed parallel to the rolling direction and the LSP treatment of a 5×5 mm area was applied on the surface afterwards, as shown in Fig. 12. In total 10 specimens were LSP investigated. Results of the fatigue crack propagation test are summarized in Table 2. The LSP treatment led to a significantly higher number of cycles required for propagating the fatigue crack to failure. The maximum fatigue life extension was by a factor of 4.9±2.6 in comparison with the base material.

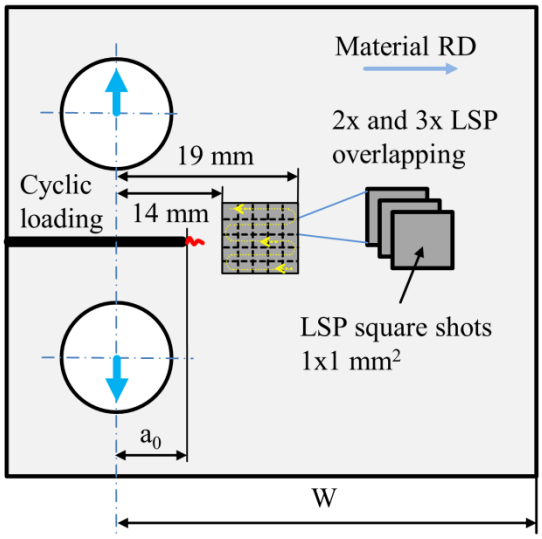

Fig. 12 C(T)50 specimen for measurement of fatigue crack propagation after LSP treatment. $a_0 = 10$ mm, $W = 50$ mm, pre-crack 2 mm, LSP area 5×5 mm

Table 2 Results of the fatigue crack propagation test

Specimen name	**LSP parameters**			**Number of cycles to failure**	**Life extension,** number	**Pre-crack,** mm
	Optics, mm	**Energy,** J	**Overlap,** number			
Base material	-	-	-	73000	-	2
LSP 3.1J 3× 1				259000	3.5	
LSP 3.1J 3× 2				134000	1.8	
LSP 3.1J 3× 3	1	3.1	3	185000	2.5	2
LSP 3.1J 3× 4				160000	2.2	
LSP 3.1J 3× 5				127000	1.7	
LSP 4.8J 2× 6				388000	5.3	
LSP 4.8J 2× 7				419000	5.7	
LSP 4.8J 2× 8	1	4.8	2	136000	1.9	2
LSP 4.8J 2× 9				622000	8.5	
LSP 4.8J 2× 10				216000	3.0	

The crack length a vs. number of cycles N for 10 specimens is shown in Fig. 13a). The treatment condition LSP 4.8J 2× shows an experimental scatter in the number of cycles to failure from 216,000 to 622,000 cycles, which is considerable higher than the experimental scatter from 127,000 to 259,100 cycles for treatment condition LSP 3.1J 3×. The experimental scatter in the number of cycles to failure follows the Weibull distribution for both treatment conditions as

shown in Fig. 14. The fitting lines are defined by the following equation (2-parametric Weibull distribution):

$$H = 100\% \left(1 - e^{-(N/T)^b}\right), \quad (1)$$

where H is the failure rate, N the number of cycles, T a scale parameter and b the shape parameter. For the two parameter combinations, the following parameters were obtained: $T_1 = 189502.6$, $b_1 = 3.911$ for treatment condition LSP 3.1J 3× and $T_2 = 413178.0$, $b_2 = 1.754$ for treatment condition LSP 4.8J 2×. The shape parameter b characterizes the failure rate over the number of cycles (i.e. experimental scatter) and is widely used in reliability engineering. For the given case ($b_1 > b_2 = 2.2$), it can be seen that the failure rate for the treatment condition LSP 4.8J 2× increases over the number of cycles slower than for the treatment condition LSP 3.1J 3×. By extrapolating fitting lines to the probability of failure of 10% one can see that both treatment conditions lead to comparable fatigue life extension of approx. 100000 cycles. This is due to the fact that both parameter combinations lead to the generation of residual stress profiles with comparable integral stress area. The average values for the integral stress area with standard deviation obtained from eight residual stress measurements for each treatment condition are summarized in Table 3. The treatment conditions LSP 4.8J 2× and 3.1J 3× lead to comparable average values of integral stress area but with considerable different standard deviation. The experimental scatter in fatigue life data can be explained by experimental variation (standard deviation) of the residual stress area induced by LSP treatment.

Table 3 Statistical values of integral stress area

LSP treatment condition	**Mean (average),** MPa mm	**Standard deviation,** MPa mm
LSP 4.8J 2×	184	37
LSP 3.1J 3×	176	12

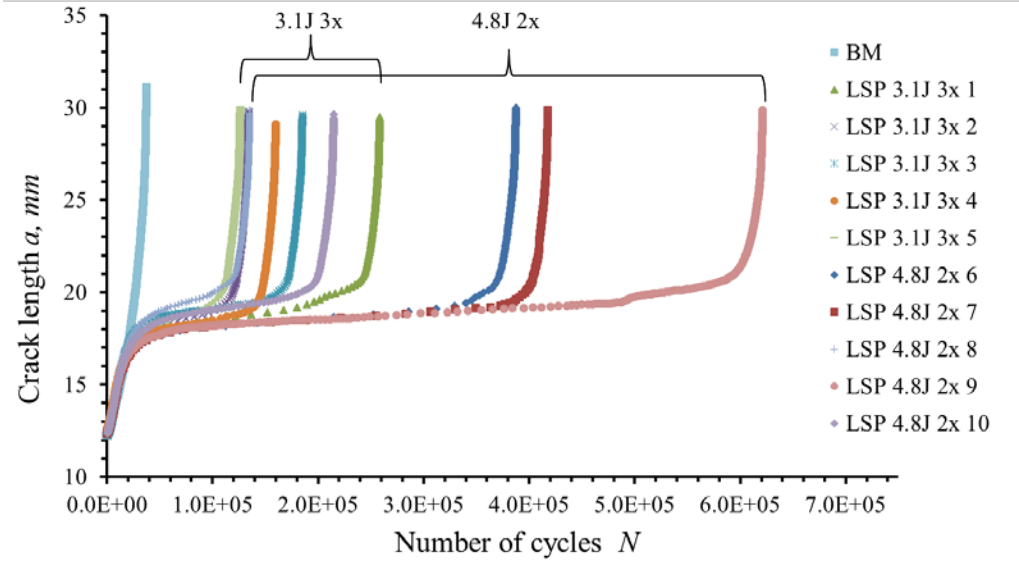

(a)

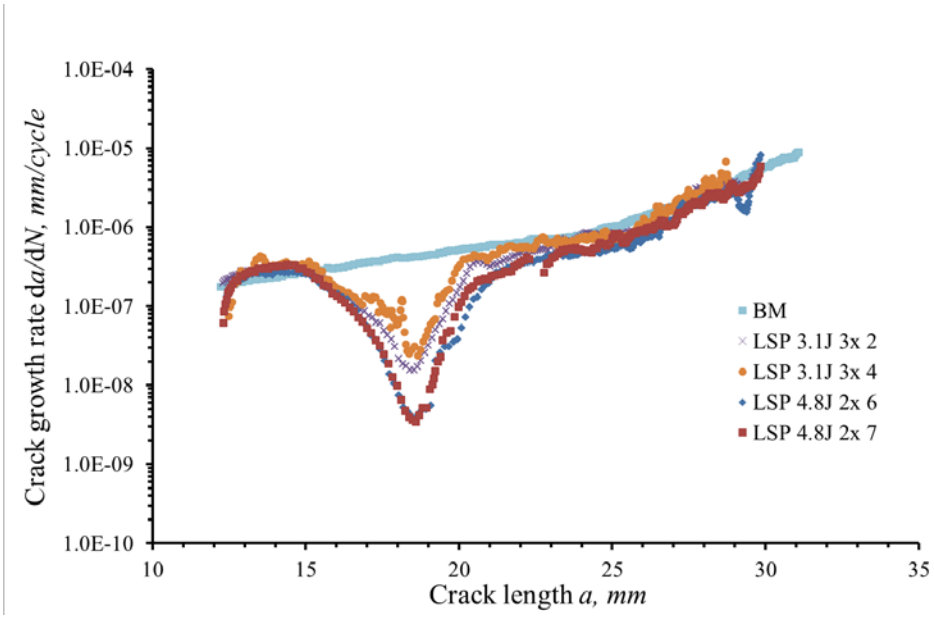

(b)

Fig. 13 Fatigue crack propagation results: (a) crack length a vs. number of cycles N, (b) crack growth rate da/dN vs. crack length a.

In Fig. 13b), the crack growth rate $\mathrm{d}a/\mathrm{d}N$ versus the crack length a is presented for four typical LSP treated specimens and is compared to the behavior of the base material. Analogous to the results obtained by Kashaev et al. [53], the LSP treated specimens indicate slightly higher $\mathrm{d}a/\mathrm{d}N$ values compared to the base material up to a crack length a of 14 mm (approximately 10,000 cycles). This phenomenon can be explained by the presence of tensile residual stresses in front of the crack tip. As the crack enters the LSP area, the crack growth rate $\mathrm{d}a/\mathrm{d}N$ decreases rapidly and reaches its minimum at approximately a = 18.5 mm. The significant mitigation of the

fatigue crack propagation is clearly attributed to the presence of the deep compressive residual stresses in the treated area, which cause crack closure under cyclic loading [18, 53, 54]. As the crack exits the LSP area at a = 19.0 mm, the crack growth rate $\mathrm{d}a/\mathrm{d}N$ is approaching the BM curve because of the release of the tensile residual stresses in the surrounding area of the LSP treated area. The crack growth rate finally reaches the level of the base material specimens at a crack length a of 21 – 22 mm.

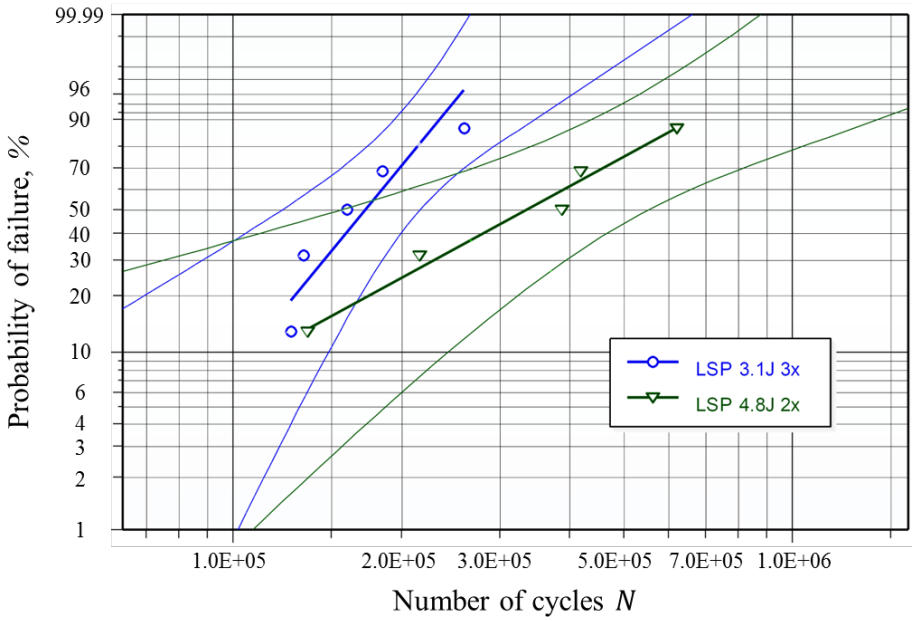

Fig. 14 Weibull distribution for fatigue life data corresponding to 3.1J 3× and 4.8J 2× treatment conditions.

5. Conclusions

The optimization of LSP process parameters (*energy*, *overlaps*, *optics*) with respect to the generated residual stress profiles was conducted by employing the statistical methods of DOE. Characteristic quantities describing the residual stress profile and which potentially affect the fatigue behavior were used as optimization variables: s*tress at 0.01 mm*, *maximum stress* and the *stress area*. The achieved results are summarized as follows:

1. The number of *overlaps* and the laser pulse *energy* have almost equal main effects and little interaction effect on stress quantities and, therefore, on residual stress profiles. This means that the *overlap* and *energy* can be inverse proportionally varied in order to achieve desired stress profiles, keeping the *optics* constant. The factor *optics* affects the s*tress at 0.01 mm* twice as strong than the factors *energy* and *overlap*.
2. The feasible region of LSP parameter variations, which leads to defined ranges of the stress quantities — *stress at 0.01 mm* < −100 MPa, *maximum stress* < −300 MPa, *stress*

area < −250 MPa mm —, was obtained within the defined process window. It is found that the highest effort is required for achieving the defined *stress at 0.01 mm* compared to other stress quantities and is only possible when 1×1 mm *optics* is used. According to the feasible region, one can operate with minimum *energy* of 3.1 J and three times *overlaps* or maximum *energy* of 4.8 J and two times *overlaps*. It is commercially more profitable to work with the laser energy of 3.1 J because the laser price is smaller in comparison with the lasers operating at the energy of 5.0 J. However, the increase in the number of *overlaps* from two to three raises the processing time by a factor of 1.5.

3. After the correction of the plasticity effect in hole drilling measurements using the artificial neural network methodology [1], the minimum compressive *maximum stress* increases from −359 MPa to −332 MPa and the minimum *stress area* increases from −298 MPa mm to −265 MPa mm; while *stress at 0.01 mm* remains unchanged. It is revealed, that the generated residual stresses measured by the hole drilling technique require a correction when the following LSP parameter levels are exceeded: 3J *energy*, 2 times *overlaps*, 1×1 mm *optics*.
4. Significant retardation of the fatigue crack growth in the LSP-treated area due to the compressive residual stresses leads to the fatigue life extension in average up to a factor of 4.9 and up to a factor of 8.5 as maximum. Two process parameter combinations: *energy* of 3.1 J and three times *overlap* (P_1), e*nergy* of 4.8 J and two times *overlap* (P_2) can be used for minimum fatigue life extension of approx. 100000 cycles because they generate residual stress profiles with comparable integral stress area. The experimental scatter in the number of cycles to failure follows the Weibull distribution which qualitatively correlates with the standard deviation of the integral stress area.

Acknowledgements

The authors wish to thank S. Riekehr and R. Dinse from Helmholtz-Zentrum Geesthacht for their valuable support in carrying out LSP experiments and L. Moura for helping with hole drilling measurements.

Declaration of conflicting interests

The authors declare that there is no conflict of interest.

Funding

This research received no specific grant from any funding agency in the public, commercial, or not-for-profit sectors.

Bibliography

[1] Ding K, Ye L (2006) Laser shock peening. Performance and process simulation. Woodhead Cambridge

[2] McElhone M, Rugg D (2005) Experimental evaluation of the fatigue performance of aero-engine fan blade dovetails. In: Presentation for the AeroMat

[3] Heckenberger U, Hombergsmeier E, Bestenbostel W, Holzinger V (2010) LSP to improve the fatigue resistance of highly stressed AA7050 components. In: Presentation for the 2nd International Conference on Laser Peening, pp 1-27

[4] Hatamleh O, Lyons J, Forman R (2007) Laser and shot peening effects on fatigue crack growth in friction stir welded 7075-T7351 aluminium alloy joints. International Journal of Fatigue 29(3):421-434

[5] Hatamleh O (2009) A comprehensive investigation on the effects of laser and shot peening on fatigue crack growth in friction stir welded AA2195 joints. International Journal of Fatigue 31(5):974-988

[6] Zhao J, Dong Y, Ye C (2017) Laser shock peening induced residual stresses and the effect on crack propagation behavior. International Journal of Fatigue 100(1):407-417

[7] Rubio-Gonzalez C, Felix-Martinez C, Gomez-Rosas G, Ocana JL, Morales M, Porro JA (2011) Effect of laser shock processing on fatigue crack growth of duplex stainless steel. Materials Science and Engineering: A 528(3):914-919

[8] McClung RC (2007) A literature survey on the stability and significance of residual stresses during fatigue. Fatigue & Fracture of Engineering Materials & Structures 30(3):173-205

[9] Peyre P, Fabbro R, Merrien P, Lieurade H (1996) Laser shock processing of aluminium alloys. Application to high cycle fatigue behaviour. Materials Science and Engineering: A 210(1-2):102-113

[10] Mostafa AM, Hameed MF, Obayya SS (2017) Effect of laser shock peening on the hardness of AL-7075 alloy. Journal of King Saud University – Science, in Press

[11] United States Patent 7137282, Laser shock peening, Rolls-Royce plc http://www.freepatentsonline.com/7137282.html. Accessed 31 January 2018

[12] Sano Y, Akita K, Masaki K, Ochi Y, Altenberger I, Scholtes B (2006) Laser Peening without Coating as a Surface Enhancement Technology. Journal of Laser Micro/Nanoengineering 1(3):161-166

[13] Laser Peening (2017) Metal Improvement Company LLC. http://www.kugelstrahlen-shotpeening-mic.de/laser-peening.html. Accessed 27 October 2017

[14] Laser Peening System for Superior Metal Enhancement, Metal Forming, Fatigue and Cracking Prevention (2014) LSP Technologies Inc. https://www.lsptechnologies.com/. Accessed 24 October 2017

[15] MacGillivray K, Dane B, Osborne M, Bair R, Garcia W (2010) F-22 Laser Shock Peening Depot Transition and RiskReduction. In: USAF ASIP Conference, San Antonio

[16] Correa C, Ruiz de Lara L, Diaz M, Porro JA, Garcia-Beltran A, Ocana JL (2015) Influence of pulse sequence and edge material effect on fatigue life of Al2024-T351 specimens treated by laser shock processing. International Journal of Fatigue 70:196-204

[17] Bhamare S, Ramakrishnan G, Mannava SR, Langer K, Vasudevan VK (2013) Simulation-based optimization of laser shock peening process for improved bending fatigue life of Ti–6Al–2Sn–4Zr–2Mo alloy. Surface and Coatings Technology 232:464-474

[18] Sheng J, Huang S, Zhou J, Xu S, Zhang H (2016) Effect of laser peening with different energies on fatigue fracture evolution of 6061-T6 aluminum alloy. Optics & Laser Technology 77:169-176

[19] Zabeen S, Preuss M, Withers P (2015) Evolution of a laser shock peened residual stress field locally with foreign object damage and subsequent fatigue crack growth. Acta Materialia 83:216-226

[20] You C, Achintha M, He B, Reed P (2017) A numerical study of the effects of shot peening on the short crack growth behaviour in notched geometries under bending fatigue tests. International Journal of Fatigue 103:99-111

[21] Frija M, Sghaier RB, Bouraoui C and Fathallah R (2012) Optimizing Residual Stress Profile Induced by Laser Shock Peening Using DOE Technique. Applied Mechanics and Materials 146:83-95

[22] Sibalija TV, Petronic SZ, Majstorovic VD, Milosavljevic A (2014) Modelling and optimisation of laser shock peening using an integrated simulated annealing-based method. The International Journal of Advanced Manufacturing Technology 73:1141-1158

[23] Sokol D, Clauer A, Ravindranath R, Lahrman DF (2004) Applications of Laser Peening to Titanium Alloys. In: ASME/JSME 2004 Pressure Vessels and Piping Division Conference, San Diego, CA

[24] Achintha M, Nowell D, Fufari D, Sackett EE, Bache MR (2014) Fatigue behaviour of geometric features subjected to laser shock peening: Experiments and modelling. International Journal of Fatigue 62:171-179

[25] Braisted W, Brockman R (1999) Finite element simulation of laser shock peening. International Journal of Fatigue 21(7):719-724

[26] Keller S, Chupakhin S, Staron P, Maawad E, Kashaev N, Klusemann B (2018) Experimental and numerical investigation of residual stresses in laser shock peened AA2198. Journal of Materials Processing Technology 255:294-307

[27] Hfaiedh N., Peyre P, Song H, Popa I, Ji V, Vignal V (2015) Finite element analysis of laser shock peening of 2050-T8 aluminum alloy. International Journal of Fatigue 70:480-489

[28] Cellard C, Retraint D, Francois M, Rouhaud E and Saunier D (2012) Laser shock peening of Ti-17 titanium alloy: Influence of process parameters. Materials Science and Engineering A 532:362-372

[29] Warren A, Guo Y, Chen S (2008) Massive parallel laser shock peening: Simulation, analysis, and validation. International Journal of Fatigue 30:188-197

[30] Ebrahimi M, Amini S, Mahdavi S (2017) The investigation of laser shock peening effects on corrosion and hardness properties of ANSI 316L stainless steel. The International Journal of Advanced Manufacturing Technology 88(5):1557-1565

[31] Kamkarrad H, Narayanswamy S, Keshmiri M (2015) High repetition laser shock peening on magnesium based biodegradable alloys. Journal of Laser Micro/Nanoengineering 10(3):291-297

[32] Trdan U, Ocana J, Grum J (2011) Surface modification of aluminium alloys with laser shock processing. Journal of Mechanical Engineering 57(5):385-393

[33] ASM Aerospace Specification Metals Inc, Aluminum 2024-T3. http://asm.matweb.com/search/SpecificMaterial.asp?bassnum=MA2024T3. Accessed 28 February 2017

34] Huda Z, Taib NI, Zaharinie T (2009) Characterization of 2024-T3: An aerospace aluminum alloy. Materials Chemistry and Physics 113(2-3):515-517

[35] DeGarmo EP, Black JT, Kohser RA (2003) Materials and processes in manufacturing 9th ed, John Wiley & Sons Inc, New York

[36] Kacar H, Atik E, Meric C (2003) The effect of precipitation-hardening conditions on wear behaviours at 2024 aluminium wrought alloy. Journal of Materials Processing Technology 142(3):762-766

[37] Enz J, Khomenko V, Riekehr S, Ventzke V, Huber N, Kashaev N (2015) Single-sided laser beam welding of a dissimilar AA2024–AA7050 T-joint. Materials & Design 76:110-116

[38] Chupakhin S, Kashaev N, Klusemann B, Huber N (2017) Artificial neural network for correction of effects of plasticity in residual stress profiles measured by hole drilling. The Journal of Strain Analysis for Engineering Design 52(3):137-151

[39] American Society for Testing and Materials (ASTM) (2008) Standard test method for determining residual stresses by the hole-drilling strain-gage method, standard test method E837-08. American Society for Testing and Materials, West Conshohocken, PA

[40] Measurements Group (2001) Measurement of residual stresses by hole-drilling strain gage method. Tech note TN-503-6, Vishay Measurements Group, Raleigh, NC

[41] Grant PV, Lord JD, Whitehead PS (2002) The measurement of residual stresses by the incremental hole drilling technique. Measurement good practice guide 53, National Physical Laboratory, UK

[42] Steinzig M, Ponslet E (2003) Residual stress measurement using the hole drilling method and laser speckle interferometry: part 1. Experimental techniques SEM 27(3):43-46

[43] Beghini M, Bertini L, Santus C (2010) A procedure for evaluating high residual stresses using the blind hole drilling method, including the effect of plasticity. Journal of Strain Analysis for Engineering Design 45(4):301-318

[44] Chupakhin S, Kashaev N, Huber N (2016) Effect of elasto-plastic material behaviour on determination of residual stress profiles using the hole drilling method. The Journal of Strain Analysis for Engineering Design 51(8):572-581

[45] Jeff Wu CF (2000) Experiments. Planning, analysis, and parameter design optimization. John Wiley and Sons, New York

[46] Montgomery D C (2001) Design and analysis of experiments, 5th ed., John. Wiley & Sons, New York

[47] Box GE, Hunter WG, Hunter JS (1978) Statistics for experimenters. John Wiley & Sons, New York

[48] Meeker WQ, Escobar LA (1998) Statistical methods for reliability data. John Wiley & Sons, New York

[49] ReliaSoft (2014) User's guide DOE++. ReliaSoft Publishing

[50] ReliaSoft Corporation (2015) Experiment design & analysis reference. ReliaSoft Publishing, Tucson

[51] Wu CFJ, Hamada M (2000) Experiments: planning, analysis and parameter design optimization. John Wiley & Sons, New York

[52] ReliaSoft Corporation (2015) Quick start guide. ReliaSoft Publishing, Tucson

[53] Kashaev N, Ventzke V, Horstmann M, Chupakhin S, Riekehr S, Falck R, Maawad E, Staron P, Schell N, Huber N (2017) Effects of laser shock peening on the microstructure and fatigue crack propagation behaviour of thin AA2024 specimens. International Journal of Fatigue 98:223-233

[54] Ge M-Z, Xiang J-Y (2016) Effect of laser shock peening on microstructure and fatigue crack growth rate of AZ31B magnesium alloy. Journal of Alloys and Compounds 680:544-552

Appendix

Table 4 Summary of designed experiments

Number of experiments	**Run order**	**A: Optics,** mm	**B: Overlap,** number	**C: Energy,** J	***Stress area,*** MPa mm	***Stress at 0.01 mm,*** MPa	***Maximum stress,*** MPa
1	39	1	1	1.3	−160	24	−201
2	48	1	1	1.3	−155	23	−181
3	53	1	1	1.3	−262	−71	−304
4	1	1	2	1.3	−231	−46	−271
5	11	1	2	1.3	−219	−29	−300
6	13	1	2	1.3	−151	−3	−168
7	18	1	3	1.3	−271	−81	−374
8	37	1	3	1.3	−251	−43	−300
9	44	1	3	1.3	-	-	-
10	19	1	1	3	−210	−7	−258
11	21	1	1	3	-	-	-
12	24	1	1	3	−220	−34	−304
13	4	1	2	3	−313	−116	−411
14	29	1	2	3	-	-	-
15	34	1	2	3	−291	−70	−390
16	9	1	3	3	−161	−2	−214
17	17	1	3	3	−302	−143	−384
18	22	1	3	3	−298	−120	−371
19	6	1	1	5	−220	−46	−289
20	14	1	1	5	−204	−17	−275
21	33	1	1	5	-	-	-
22	45	1	2	5	−298	−149	−365
23	47	1	2	5	−280	−108	−359
24	54	1	2	5	−303	−164	−398
25	12	1	3	5	−300	−197	−321
26	31	1	3	5	−294	−117	−382
27	35	1	3	5	−260	−78	−310
28	5	3	1	1.3	7	51	41
29	7	3	1	1.3	7	51	41
30	30	3	1	1.3	7	51	41
31	16	3	2	1.3	7	51	41
32	42	3	2	1.3	7	51	41

Table 4 Summary of designed experiments

Number of experiments	**Run order**	**A: Optics,** mm	**B: Overlap,** number	**C: Energy,** J	***Stress area,*** MPa mm	***Stress at 0.01 mm,*** MPa	***Maximum stress,*** MPa
33	52	3	2	1.3	7	51	41
34	8	3	3	1.3	7	51	41
35	50	3	3	1.3	7	51	41
36	51	3	3	1.3	7	51	41
37	2	3	1	3	−43	43	−31
38	20	3	1	3	−65	59	−52
39	38	3	1	3	−54	52	−51
40	3	3	2	3	−93	10	−110
41	27	3	2	3	−78	63	−96
42	41	3	2	3	−100	19	−128
43	28	3	3	3	−96	−5	−122
44	40	3	3	3	−103	13	−126
45	49	3	3	3	−82	80	−103
46	10	3	1	5	−80	21	−111
47	23	3	1	5	−74	89	−97
48	43	3	1	5	−102	−18	−118
49	26	3	2	5	−144	−4	−200
50	32	3	2	5	−172	−31	−223
51	46	3	2	5	−163	−10	−194
52	15	3	3	5	−202	−25	−252
53	25	3	3	5	−233	−13	−299
54	36	3	3	5	−180	−38	−222

Table 5 Summary of designed experiments which required correction

Number	**Run order**	**Optics,** mm	**Overlap, number**	**Energy,** J	**Stress area,** MPa mm		**Stress at 0.01 mm,** MPa		**Maximum stress,** MPa	
					Orig.	Corr.	Orig.	Corr.	Orig.	Corr.
1	4	1	2	3	−313	−274	−116	−116	−411	−357
2	34	1	2	3	−291	−270	−70	−70	−390	−362
3	17	1	3	3	−302	−274	−143	−143	−384	358
4	22	1	3	3	−298	268	−120	−120	−371	−347
5	45	1	2	5	−298	−271	−149	−149	−365	−351
6	47	1	2	5	−280	−254	−108	−108	−359	−345
7	54	1	2	5	−303	−275	−164	−164	−398	−362
8	12	1	3	5	−300	−272	−197	−197	−321	−310
9	31	1	3	5	−294	−269	−117	−117	−382	−341
10	35	1	3	5	−260	−237	−78	−78	−310	−303